



Geomorphological mapping for liquefaction likelihood: the Piniada Valley case study (central Greece)

S. Valkaniotis¹ · D. Rapti² · M. Taftoglou¹ · G. Papathanassiou³ · R. Caputo⁴

Received: 22 March 2024 / Accepted: 1 August 2024 / Published online: 12 August 2024
© The Author(s) 2024

Abstract

Assessment of liquefaction susceptibility of sediments in alluvial plains is considered one of the first step for infrastructure planning, hazard mitigation, and land use management in seismically active regions. Subtle geomorphological features resulting from depositional processes could greatly contribute to estimating the liquefaction likelihood since they also dictate the type and distribution of sediments. Our case study is from the Piniada Valley (Greece), where widespread liquefaction phenomena were triggered by the 2021 Mw 6.3, Damasi earthquake. As we compiled a detailed geological map for the purposes of this investigation and correlated it to the spatial distribution of the earthquake-induced liquefaction phenomena, we observed that most of liquefaction surface evidence are related to point bars and abandoned river channels formed the last century. In particular, the areal liquefaction density was estimated at 60.7 and 67.1 manifestations per km², for the point bars and abandoned channels, respectively. Following this outcome, we propose a refinement of the existing liquefaction susceptibility classifications by including point bar bodies as a distinct category, characterized by a very high susceptibility to liquefaction. In addition, we discuss the correlation between the observed liquefaction manifestations and the shallow lithofacies, sand or mud prone areas, within point bars. The outcome arisen by this research is that most of liquefaction phenomena (> 70%) occurred on the area covered by coarser materials deposited on the upstream part of high sinuosity meanders.

Keywords Point bars · Liquefaction · Fluvial · Susceptibility · Earthquake

✉ D. Rapti
cpr@unife.it

¹ Department of Civil Engineering, Democritus University of Thrace, Xanthi, Greece

² Department of Chemical, Pharmaceutical and Agricultural Sciences, Ferrara University, Ferrara, Italy

³ School of Geology, Aristotle University of Thessaloniki, Thessaloniki, Greece

⁴ Department of Physics and Earth Sciences, Ferrara University, Ferrara, Italy

1 Introduction

Liquefaction encompasses a range of phenomena induced by earthquakes, where the strength and stiffness of a soil deposit are reduced due to the generation of pore water pressure (Youd 1993). Liquefaction consequences can range from minor settlements and lateral spreading to substantial flow slides involving horizontal and vertical displacements measured in tens of meters (Kramer 2008). Consequently, liquefaction has the potential to lead to foundation and retaining structure settlements and tilts, or even substantial differential displacements causing damages not only to surface structures like buildings and bridges, but also to geotechnical structures such as river embankments, foundations and retaining walls, as well as to critical infrastructure including runways, port facilities and other underground infrastructure such as gas pipelines, water mains, and sewage systems (Hamada and O'Rourke 1992; O'Rourke and Hamada 1992; Tokimatsu et al. 2019), even for moderate earthquakes (Galli 2000; Papathanassiou et al. 2005; Papathanassiou and Pavlides 2011). Therefore, liquefaction triggered by earthquakes can pose serious security issues for critical infrastructure.

Studying the liquefaction triggering as part of an earthquake protection strategy is a multiparameter task. At a local scale, it is well known that laboratory testing of soil samples should be conducted aiming to examine the grain size analysis and Atterberg limits of the material (e.g., Wang 1979, Seed and Idriss 1982; Andrews and Martin 2000; Polito and Martin 2001; Seed et al. 2003; Bray and Sancio 2006; Boulanger and Idriss 2006). Having assessed the susceptibility to liquefaction, then the factor of safety per soil layer can be computed based on data provided by in-situ tests, mainly SPT and CPT (Youd et al. 2001; Idriss and Boulanger 2008; Boulanger and Idriss 2014; Moss and Chen 2008; Cetin et al. 2004). Assessment of liquefaction susceptibility of soil layers on a regional scale is commonly based on qualitative or semi-quantitative approaches, mainly developed during the second half of the twentieth century. The criteria used for the classification of sediments that are prone or not to liquefaction were generally correlated to basic characteristics of the geomorphological environment. The most applied and well-known criteria are the ones proposed by Youd and Perkins (1978), Wakamatsu (1992) and Wakamatsu et al. (2001).

These classifications were largely applied in the past by geologists and engineers and are still quite popular for defining the likelihood of shallow granular deposits to liquefy and consequently to “host” liquefaction-induced failures either in free field conditions or built environment (Papathanassiou et al. 2010; Bozzoni et al. 2021; Taftsoğlu et al. 2022; Meisina et al. 2022). Highlighting the most susceptible areas covered by the relevant type of deposits is considered as a basic step for avoiding interfering with the most hazardous locations and/or for mitigating the expected failures. In both cases, forecasting of liquefaction occurrences is a procedure that enhances the seismic resilience of the community.

During the last decade and especially following some major earthquakes associated with diffuse secondary seismic effects, researchers started realizing that the triggering of liquefaction clustering phenomena seems to follow defined patterns. This preferential behaviour of the sediments to produce liquefaction manifestations was intensively investigated in some notable event occurred in New Zealand, Italy, Greece and Turkey (Wotherspoon et al. 2012; Di Manna et al. 2012; Galli et al. 2012; Bastin et al. 2015; Papathanassiou et al. 2012, 2015, 2022; Civico et al. 2015; Taftsoğlu et al. 2023; Abayo et al. 2023 among others).

In several cases, it was concluded that most of the liquefaction phenomena were not randomly distributed over an apparently uniform floodplain. Specific geomorphological areas

within fluvial meandering systems such as old/abandoned channels, point bars and oxbow lakes or reclaimed land certainly favoured their occurrences, showing a higher liquefaction density compared to other sectors of the same floodplain. Accordingly, it is becoming a common need among the scientific community to update the existing classifications by introducing the significance (and the importance) of a detailed geological and geomorphological mapping for characterizing the different sectors of a floodplain in terms of differential geotechnical behaviour of the shallow subsoil. The reliability of such liquefaction susceptibility maps would largely benefit of this approach and the present note wants to contribute to this aim.

In order to achieve this goal, it is crucial to include in any geotechnical study to be conducted in an earthquake prone area an additional task purposely devoted to compiling a geomorphologically constrained geological map. In most cases, such investigation could take advantage on data that can be retrieved from open-access repositories or collected by official agencies such as historical topographic maps, geological maps, vintage aerial imagery (before major human impact) and more recent satellite imageries. A careful processing of these data will potentially enable to retrieve the evolution of the fluvial environments within the alluvial plain and consequently to map in detail and classify the different geomorphological and sedimentological units.

Following the compilation of a detailed geological map of the Piniada Valley, this study examined the refinement of the classification proposed by Youd and Perkins (1978) in terms of type and age of grouped deposits. We quantitatively investigated the relation between point bar, flood plain and abandoned river channel deposits with respect to liquefaction manifestations based on data provided by the field survey of the 2021, Damasi, Greece Mw 6.3 earthquake (Papathanassiou et al. 2022). Our study focused on the heterogeneity of the material accumulated on the inner part of a meander, i.e. point bar deposits, aiming to examine the correlation between the distribution of sand- and mud-rich deposits and the density of liquefaction phenomena. In order to achieve this goal, we applied the method proposed by Russell et al. (2018) to four point bars in order to delineate the distribution of the two predominant lithofacies. Although this approach is considered as simplified relative to the complexity and the dynamic of a meander evolution, our study shows that its application can contribute to recognize and delimit in detail liquefaction hazardous zones within a point bar geomorphological feature.

2 Geological framework

The broader Aegean Region is characterized by an important seismic activity, which also involves large sectors of continental Greece including Thessaly (Caputo and Pavlides 1993), where starting on March 3rd, 2021, an important seismic sequence occurred (Fig. 1). It was characterized by a couple of major events (M_w 6.0 and 6.3) and 5–6 moderate ones ($M_w > 5.0$) followed by several months of aftershocks (Chatzipetros et al. 2021; Kassaras et al. 2022; Kaviris 2023; Papadimitriou et al. 2023). The epicentral area was roughly delimited by Tyrnavos, Elassona and Zarkos villages and diffuse damage occurred in a number of minor settlements within the Antichasia Mountains (Fig. 1). Satellite geodesy (Tolomei et al. 2021; De Novellis et al. 2021; Ganas et al. 2021; Papadimitriou et al. 2023) and relocated seismicity (Karakostas et al. 2021; Michas et al. 2021) indicate that the seismogenic sources were blind and rupture did not breach the surface (Caputo 2005). These seismogenic sources were not mapped and/or their tectonic features were not

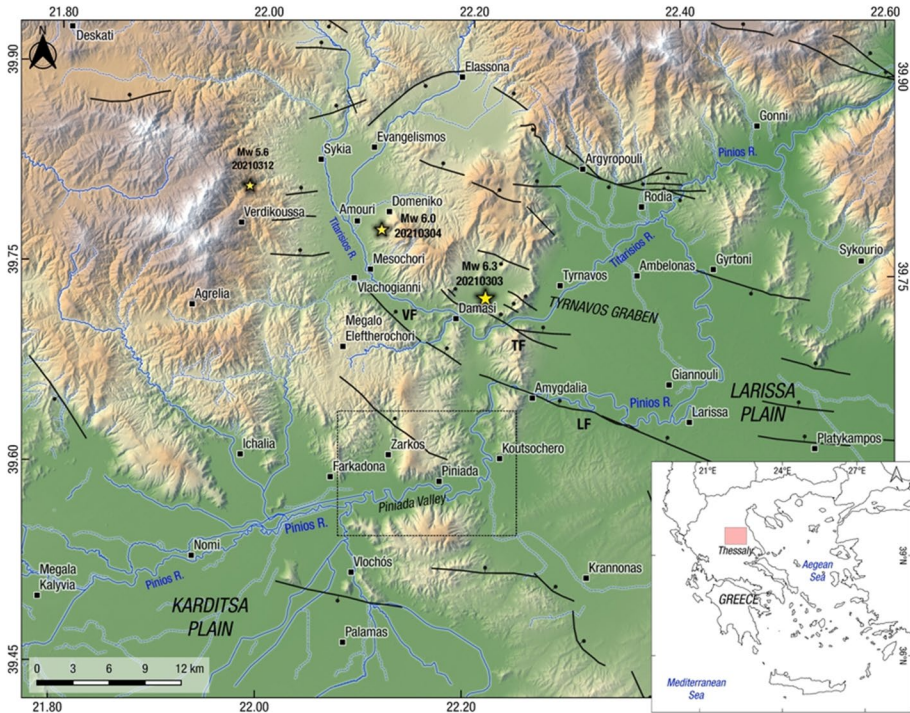


Fig. 1 Map with the principal morphological and tectonic features characterizing Thessaly, showing the location of the largest 2021 Damasi events (stars). The black box indicates the area represented in Fig. 5. TF: Tyrnavos fault, LF: Larissa fault, VF: Vlachogianni fault

classified as active (Caputo 1990, 1995; Chatzipetros et al. 2021; Ganas et al. 2021; Koukouvelas et al. 2021, 2023).

The activity of the Tyrnavos Graben has played a crucial role in the Quaternary geological evolution of the whole Thessalian region (Caputo 1990, 1995; Caputo et al. 1994). Indeed, the hydrographic network of the Pinios River clearly shows some major anomaly as far as the Karditsa and Larissa basins, characterized by two distinct endhoreic hydrographic networks up to early Quaternary, have been only recently connected along the Piniada Valley (Caputo et al. 2021). Geophysical analyses (Mantovani et al. 2018) suggest a palaeo-valley bottom sloping from north-to-west, in an opposite direction with respect to the present-day Pinios River flow. Up to Middle Pleistocene this valley likely represented the lower reach of the Titarissios River, but it was abandoned due to its tectonically induced deviation into the Larissa Basin. The progressive sedimentary aggradation of the Piniada Valley during Late Quaternary finally caused its partial infilling up to a morphological threshold in its eastern sector, the Kalamaki Gorge (Caputo et al. 2021).

The alluvial plain of the Piniada Valley is covered by fluvial deposits, basically sand and coarse silt. In reality, the thickness of the clastic layers is limited to the shallowest part of the Upper Pleistocene to Holocene sedimentary succession infilling the Piniada Valley (Caputo et al. 2022). This has been well documented by a 62 m-deep core drilled in the middle of the plain southwest of Zarkos village showing silt–clay deposits prevailing up to ca. 23 m and coarse-grain sandy layers (sometimes up to fine gravels) instead dominating

upwards (Fig. 2) clearly confirming the forementioned environmental change in time. In particular, taking into account the available ages along the core, a typical fluvial environment within the western sector of the Piniada Valley starts appearing only during the latest Pleistocene, though its definite establishment as it could be observed today basically occurs in a post-LGM (Last Glacial Maximum) period and mainly Holocene. Based on the reconstructed evolution (Caputo et al. 2021), it is also reasonable to assume a progressive shallowing of Holocene sediments towards the eastern sector of the valley, where most liquefaction phenomena occurred in concomitance with the 2021 Damasi earthquake.

The conceptual hydrogeological model of the alluvial plain is characterized by a complex multi-aquifer system consisting of several isolated and/or interconnected bodies.

This aquifer system consists of an unconfined or locally semi-confined multilayer shallow aquifer system (A_0) mainly developed in lens-shaped sandy bodies originating directly from past paths of the Pinios River, usually as infilling deposits of abandoned channels and meanders. These aquifers may locally be in hydraulic communication with each other and are characterized by a strong variability of hydraulic and geometric parameters along both horizontal and vertical dimensions. The main feeding occurs directly via infiltration from atmospheric precipitation and secondarily from the main course of the river laterally into the neighbouring aquifers. Also, during major flooding events, water could infiltrate directly into the subsoil. In the past, the shallowest aquifer was largely exploited using 2–3

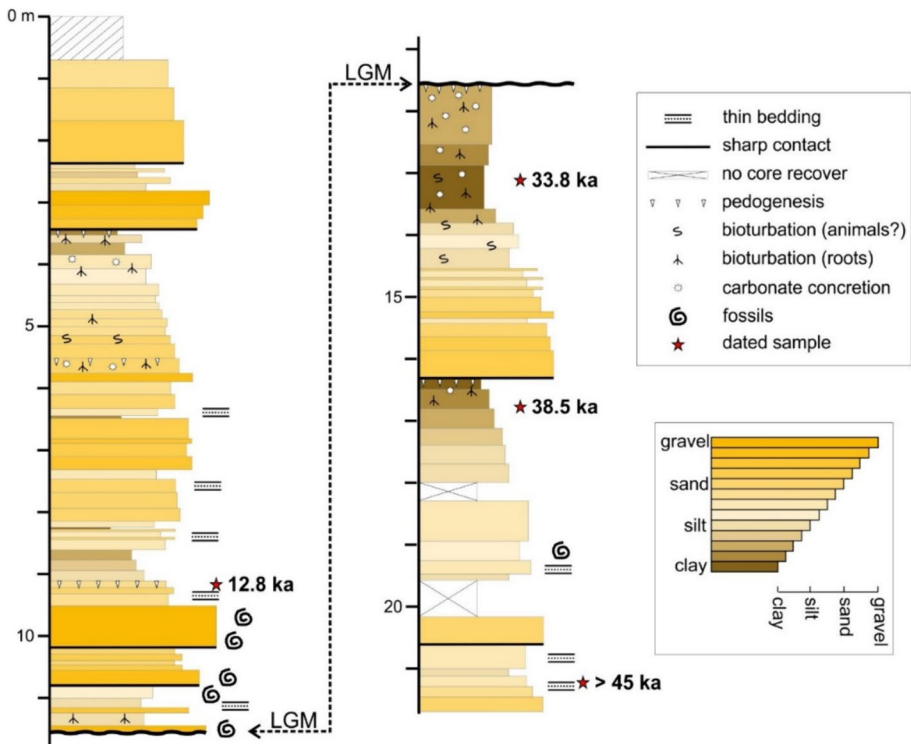


Fig. 2 Detailed vertical log from coring representing the shallowest ca. 20 m of sedimentary succession characterizing the Piniada Valley alluvial plain and showing the occurrence of several sandy layers in the first 10 m, likely prone to liquefaction. Modified from Caputo et al. (2022)

m-deep wells by the local people as a source for water supply for drinking and domestic needs. These wells have been progressively abandoned due to the high vulnerability of the aquifer to sources of surface pollution and the lowering of the piezometric level during the summer period which could locally cause the drying out of the sandy lenses. At a slightly greater depth (5–10 m) the subsoil of the Piniada Valley contains a mainly sandy confined multi-aquifer system (A), locally explored for agricultural purposes. Hydraulic communication between the first confined and the shallow unconfined aquifer could be possible. Following the construction of several small dams across the riverbed for irrigation purposes, including the reach of the river along the Piniada Valley, the height of the free water level is relatively constant during most of the year, commonly ranging at a depth of 2–4 m from the altitude of the nearby alluvial plain. Note that along the whole length of Piniada Valley, Pinios River has no natural levees, nor artificial embankments. In conclusion, at the time of the 2021 seismic events, the sandy deposits characterizing the shallow subsoil of the plain were mostly in saturated conditions and this played a crucial role during the ground shaking.

3 Methods and data analysis

The goals of this study are to compile a detailed geomorphology-based map of Holocene geology at the area of Piniada Valley and to investigate the pattern of liquefaction phenomena in terms of frequency for different geological units. It is crucial to point out that in the 1:50,000 scale geological map of the study area (Vidakis 1998), the information provided for each type of geological unit is certainly not sufficient for properly assessing the liquefaction likelihood of the sediments. This is due to the fact that liquefaction-related behaviour of a soil unit is strongly dependent on its depositional history in terms of grain size distribution, occurrence and characteristics of layering, and age. Considering that the dominant grain size of a sedimentary layer depends on the facies environment, it is evident that a detailed Holocene geomorphological and geological mapping is of outmost importance for a reliable assessment of liquefaction likelihood/susceptibility of the shallow depositional succession.

We updated a methodology for retrieving the palaeo-environmental information in an area (Taftoglou et al. 2022), that was applied on available and newly collected data from the Piniada Valley (Fig. 3). The applied method consists of three major phases: (1) data input, (2) geomorphological-based mapping and (3) estimation of the liquefaction likelihood of the deposits.

We acquired a variety of geological, historical, topographic maps and remote sensing data aiming to trace the evolution of the Piniada alluvial plain. More specifically, we used (1) the early twentieth century topographic map sheets in scale of 1:75,000 by the Royal Hellenic Army Geographical Service (1909a, b); (2) cadastral maps from the Ministry of Agriculture, dated 1928, 1929 and 1952 in scale of 1:5000; (3) aerial photographs from Hellenic Cadastre archive, acquired in 1935; (4) the 1945 orthophotomap produced by the Hellenic Army Geographical Service (2008); (5) orthorectified Corona declassified imagery of 1960 from USGS/EROS; (6) the Hellenic Army Geographical Service 1978–1980 topographic map sheets in scale of 1:5000; (7) very high resolution satellite imagery (2012–2018) from Copernicus CSCDA, (8) high resolution (10–30 m) Landsat 5/7/8 satellite imagery (1984–today) and (9) Copernicus Sentinel-2 imagery

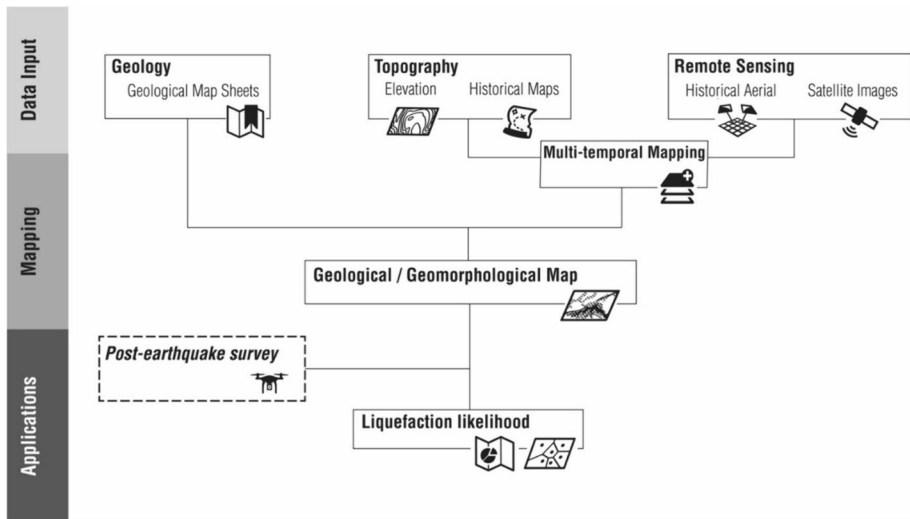


Fig. 3 Flowchart showing the phases of the method applied in this study for the compilation of geomorphological-based detailed geological map and the application to assess the liquefaction likelihood of sediments

(2015–today). Furthermore, we used a digital surface model of the study area with 5 m of spatial resolution, obtained from the Hellenic Cadastre (2007).

Using these data, it was possible tracing the different geomorphological and surficial features characterizing the Piniada Valley and assessing their relative age and type (or formation). It is worth to note that the carried-out processing of multi-temporal and historical data (Fig. 4) enables tracing and dating of features that are not clearly visible at present in the landscape. This is due to the rapid migration of fluvial features through time and the extensive land reclamation works realized during the second half of twentieth century that consequently masked in large portions of the Pinios River plain the surficial “footprint” of even recent geomorphological features along the Piniada Valley.

A further possible contribution to the aim of revealing near-surface geomorphological features within heavily reworked crop fields could be provided by using differences in image reflectance caused by soil moisture content and lithological variation of recent satellite imageries. Moreover, it is pointed out that significant and major geomorphological features can also leave a distinct signal in topography despite the temporal change of land cover.

We also used multiple Landsat and Sentinel-2 multispectral images aiming to observe and capture older and recent flood events and surficial water runoff within Pinios Valley; abandoned channels and riverbeds characterizing the valley still at as preferential surficial drainage paths of excess water during important flood events and even simple overflow of the Pinios River. A selection of recent flood snapshots affecting the Piniada Valley are included in the Supplementary Material.

On a subsequent investigation step, the results of the detailed post-earthquake survey of the 2021 Damasi event were correlated with the geomorphological-geological map in terms of liquefaction-induced surface evidence. We focused on the distribution of the different Holocene geological units, and particularly on the variable density of liquefaction phenomena per unit with the very final goal to propose a refinement of the

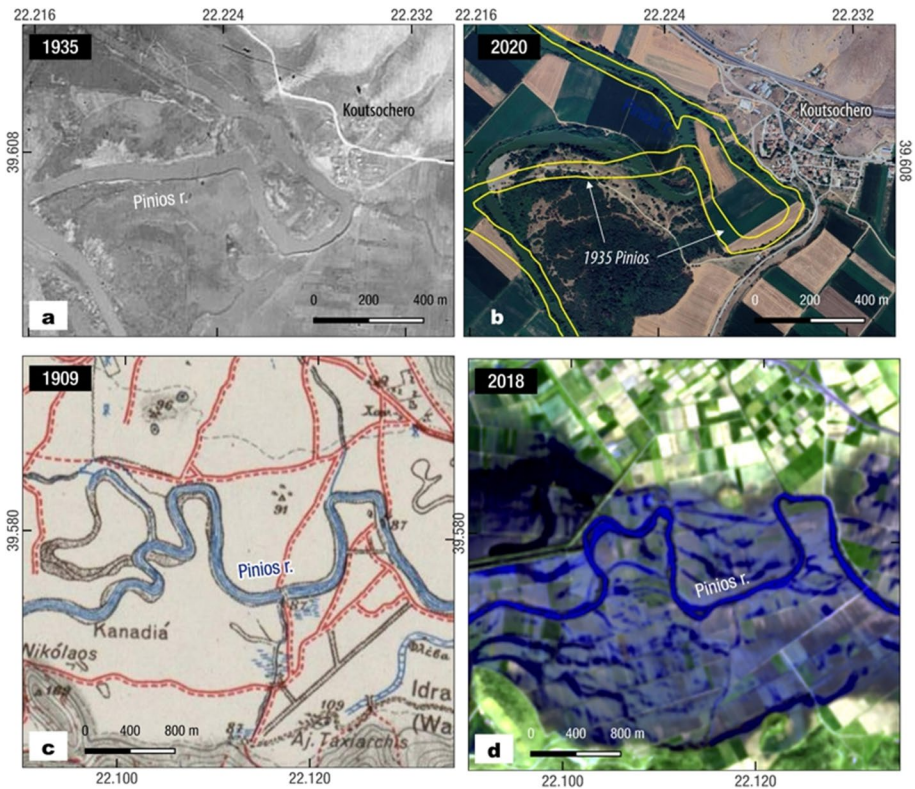


Fig. 4 **a** Historical aerial image of 1935 showing the active course of the Pinios River close to the Koutsochero settlement and comparison **b** with the present-day geometry (satellite view), where the former path clearly appears as a cut-off meander. **c** Historical topographic map of 1909 (Trikala map sheet) with the meandering course of the Pinios River near Zarko and comparison **d** with a satellite snapshot (Sentinel-2 infrared composite) of the same area during a major flooding event (March 10th, 2018); in the latter image, the river channels and the flood water are shown as dark blue colour, and areas that were flooded and retain moisture with darker shades

classification of the liquefaction likelihood, showing the importance of a good mapping for better assessing this kind of natural hazard.

4 Results

4.1 Detailed geological map of the area

The new map also contains units distinguished in terms of the sedimentary environment they represent. Accordingly, we could distinguish the following ones. Areas commonly in dry conditions, but regularly (seasonally) flooded by overflow phenomena, are referred to as floodplain surfaces. They are characterized by the finer components of the clastic materials transported by the Pinios River. These deposits consist of mainly silt and clayey silt in the more distal sector of the plain and are characterized by a sub horizontal flat upper surface. The integrated analysis of satellite imagery taken during recent flooding events and the DEM

of the area allowed to recognize and distinguish the presence of floodplain surfaces at different altitudes across the Piniada Valley thus implying a progressive abandonment (i.e. terracing) as further discussed in a following section. It is worth mentioning that in the late '40s a continuous dam embankment was constructed east of Pinios River, between Koutsochero and Kastri. As a consequence, this artificial infrastructure definitely prevented further flooding of the eastern sector of the plain, but also intense farming and heavy land manipulation largely obliterated any geomorphological evidence, thus impeding any detailed mapping.

Due to the prevailing meandering behavior of the Pinios River along the Piniada Valley, the plain is crossed by several abandoned channels. In topographic profiles, they have a typical concave upwards geometry slightly entrenched with respect to the surrounding plain. Being low topographic areas, they obviously play the role of sinks during exceptional precipitation events and in general for the overflow waters. Locally higher topographic gradients imply a greater hydraulic energy and potentially the transport of coarser deposits. Thus, trapping of sediments is enhanced due to their morphology. Consequently, abandoned channels are generally the site of an accelerated sedimentation and a relatively rapid infilling. In plan view, most of them have arc-like shapes (high sinuosity) characterized by a curvature radius varying from several hundred of meters to 50–60 m. During highly rainy periods, some of these lengthened morphological features temporarily become water ponds and in general the delay the complete drainage following an overflow event. It should be noted that some of the abandoned channels morphologically entrenching a terraced floodplain surface, especially along the right hydrographic side, lack the typical meandering geometry. Indeed, they have been attributed to a tendentially low sinuosity pattern of the fluvial system. This morphological and hydraulic change in behavior of the Pinios River has been tentatively associated with periods of increased precipitation rates, like for example the Little Ice Age (fourteenth–nineteenth centuries) or older wet climatic events. Differently from the other ones more or less tightly curved, the low sinuosity abandoned channels could also act and favour the downstream water drainage in the late stages of flooding events.

As a consequence of the meandering process characterized by a progressive lateral migration of the active channel up to its abandonment, the area of the plain standing on the inner side of the meander is the locus of a double phenomenon; firstly the complete erosion of the pre-existing deposits from the topographic surface down to the depth of the migrating channel and, secondly, the lateral aggradation with the generation of partly over posed point bars mainly consisting of medium-to-coarse-grain sediments.

A final lithological unit is represented by coarse gravels, e.g., alluvial cones produced by the secondary lateral valleys entrenching the major E-W slopes of the Piniada Valley. The uppermost part of these deposits is relatively well cemented. In plan view they show a typical fan shape geometry, while they are characterized by low-angle slope. At the toe of the cones, these deposits are systematically covered by the floodplain deposits previously described and likely continue towards the axis of the main valley with an underlying geometrical relationship. Nowadays these alluvial cones are substantially inactive as far as on top of these cones there is 1(-2) m-thick soil with a minor colluvial input (Caputo et al. 2021).

4.2 Age of the geological units

With the exception of the lateral alluvial cones, which have been attributed a post-LGM age (i.e. latest Pleistocene; see discussion in Caputo et al. (2021), all other outcropping units described above are of Holocene age.

Mainly based on historical topographic maps and historical aerial imagery, it was possible to map the channels and the meanders that were active during the twentieth century and possibly in the last few centuries. By integration with the DEM, we also reconstructed the areas developed as point bars and the coeval floodplain surfaces. All these units are at present regularly (i.e. seasonally) flooded due to overflow of the Pinios River. In the following, we refer to these units (blue colours in Fig. 5) as ‘late historical’ or class I units.

Using geomorphological, palaeo-environmental, archaeological and historical information and constraints, a relatively older set of geological units has been distinguished. In particular, a floodplain surface formed in post Neolithic (Archaic or Classical) period and possibly active up to the Ottoman period has been tentatively reconstructed (Caputo et al. 2021). Along the topographic profiles across the Piniada Valley, this surface is higher than the younger floodplain of unit I, though the difference is not sufficient to avoid water overflow in cases of major flooding. The detailed analysis of this surface also allowed to recognize the abandoned channels and the associated point bars formed during the same time window. At this regard, the above-mentioned abandoned channels which developed on this floodplain surface and associated with a braided pattern of the Pinios River likely formed during the Little Ice Age. A further difference of these channels is the entrenching depth within the coeval alluvial plain that in this case was likely shallower and hence it is likely thinner the subsequent partial sedimentary infilling. We refer to these units (green colours in Fig. 5) as ‘late Holocene-early historical’ or class II units.

Archaeological information suggests that the formation of the remaining portion of the alluvial plain occurred during Neolithic times and certainly after the lateral alluvial cones (see below). Accordingly, this undifferentiated unit (light brown in Fig. 5) is attributed to the ‘early-middle Holocene’ and referred to as class III units. We cannot exclude the possibility that some small portions of this surface are slightly older and were formed during

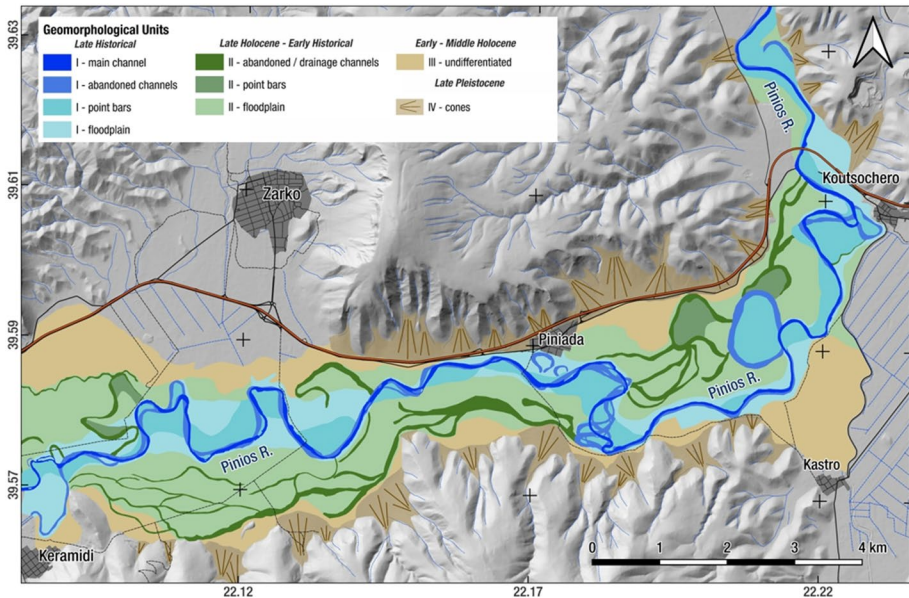


Fig. 5 Surface geological map of the Piniada Valley improved from Caputo et al. (2021). See text for detailed descriptions of mapped units

the latest Pleistocene following the LGM climatic event (*ca.* 26.5–19.5 ka BP; Clark et al. 2009).

Finally, the alluvial cone deposits produced by the secondary lateral valleys entrenching the major E-W slopes of the Piniada Valley, or at least its cemented top surface, have been attributed to the fading of LGM, say during the last 18–15 ka BP. Similar morphological features and lithological units are indeed well documented in the literature and commonly used as a chronological marker in many morphotectonic and palaeoseismological investigations (Benedetti et al. 2002; Papanikolaou et al. 2005; Caputo et al. 2006, 2010; Mason et al. 2016). Also, in a nearby site in Thessaly along the Tyrnavos Fault, radiocarbon analyses of equivalent deposits have provided ages of 19–23 ka BP (Caputo and Helly 2007) in perfect agreement with the above conclusions. In the following, these cones (brown colour in Fig. 5) are referred to as ‘late Pleistocene’ or class IV unit.

4.3 Assessing the liquefaction likelihood of the shallow deposits

To achieve this goal, we analysed the spatial distribution of the 500+ liquefaction-induced failures triggered by the 2021 Damasi earthquake (e.g., Papathanassiou et al. 2022) comparing it with our geological units (Fig. 5).

Concerning the length of the linear features, approximately 90% of the liquefaction-induced ground fissures range in dimension between 8 and 5 m, while their width varied from 0.2 to 0.8 m (Fig. 6). In addition, four large-size sand volcanoes up to 3 m in diameter and with a collapsed central crater of 0.75 m depth were created. The most impressive outcome is a strong qualitative correlation between the clustering of liquefactions with the location of palaeo-meander features and abandoned channels, as documented, for example, by historical aerial images acquired in 1945.

Having plotted the location of liquefaction sites on the geomorphological-based geological map developed by this study (Fig. 7), it is evident that most of these ground failures are concentrated on specific zones, confirming the preliminary suggestions by Papathanassiou et al. (2022). In detail, we observe that 278 cases were related to point bars, 128 to floodplain deposits, 128 to abandoned channels, and none of them to undifferentiated sediments and cones. Moreover, it was found that 379 liquefaction cases occurred on sediments referred to as late historical (class I), while 155 liquefaction cases occurred on units referred to as late Holocene-early historical (class II).



Fig. 6 Examples of liquefaction phenomena observed following the 2021 Damasi earthquake

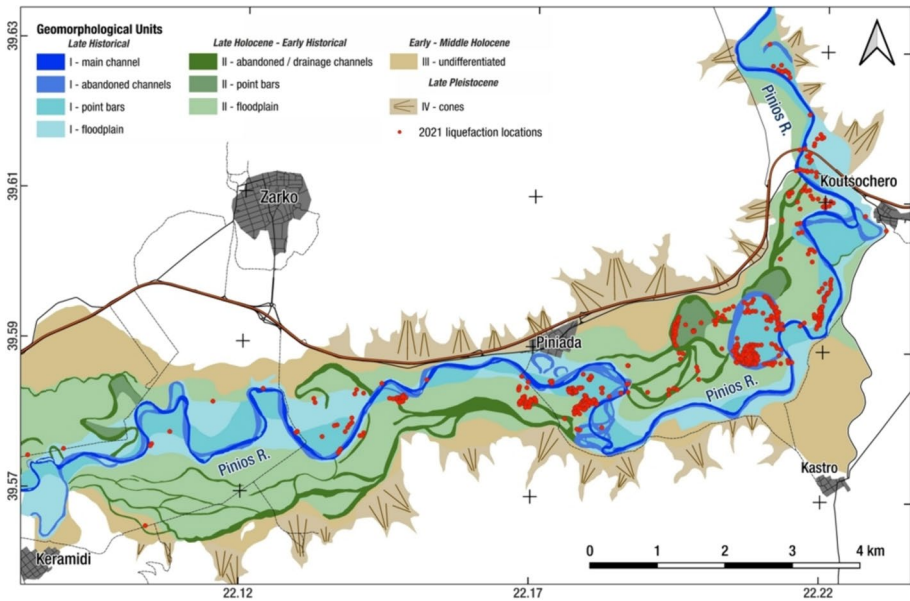


Fig. 7 Map showing the sites where liquefaction evidence (red dots) was mapped during the immediate post-event field survey

In terms of percentage, the point bars, floodplain deposits and abandoned channels of class I hosted 47.8%, 5.6% and 17.6% of the observed liquefaction cases, respectively. This outcome confirms the statement that younger sediments are looser, from poorly consolidated to unconsolidated, and consequently more likely to liquefaction if they are in saturated conditions (Youd 1998). On the other hand, older deposits, as the ones attributed to class II, cumulatively hosted a lower percentage of liquefaction manifestations. Indeed, point bars (4.3%), floodplain deposits (18.4%) and abandoned or drainage channels (6.4%), represent a total of less than 30%. The only exception to this expected outcome is that the number of liquefaction sites and the relevant percentage is lower on the younger floodplain sediments (class I) compared to the older ones (class II). Possible explanations for this are that (1) the area covered by the class II floodplain deposits is twice the area covered by the deposits of class I and consequently more cases could be statistically hosted, and (2) the floodplain deposits aged late Holocene-early historical (class II), are also geologically classified as recent ones, and characterized as very likely to liquefaction.

As far the liquefaction frequency per area (km^2) covered by the surficial sedimentary-geomorphological units (Table 1), for class I units the frequency on point bars is 60.7 manifestations per km^2 , on the floodplain deposits is 7.5 liquefaction sites/ km^2 and on the areas classified as abandoned river channels it is 67.1 liquefactions/ km^2 . In contrast, the frequency in the late Holocene-early historical sediments (class II), is 46 liquefaction phenomena per km^2 . on point bars, 9 on floodplain deposits and 15.5 in correspondence of abandoned/drainage channels. Based on these values, we can state that the difference on liquefaction frequency between floodplain deposits of class I with the ones of class II, is not as significant. This result confirms the negligible difference previously assessed on solely on the basis of the percentage of liquefaction phenomena per sedimentary-geomorphological unit. Therefore, for a more reliable analysis, it is proposed that the total area of

Table 1 Statistical analysis between the recognized geological units included in the map of Fig. 5 and associated liquefaction-induced features observed along the Piniada Valley during the immediate post-event field survey (Fig. 7)

Geological units	Area (km ²)	Liquefaction features	Liquefaction surface evidence (%)	Liquefaction density sites (km ²)
I—point bars	4.2	255	47.8	60.7
I—floodplain	4.0	30	5.6	7.5
I—abandoned channels	1.4	94	17.6	67.1
II—point bars	0.5	23	4.3	46.0
II—floodplain	10.9	98	18.4	9.0
II—abandoned/drainage channels	2.2	34	6.4	15.5
III—undifferentiated	7.1	0	0.0	0.0
IV—cones	5.1	0	0.0	0.0
Total	35.4	534	100	

Tentative ages are I: late historical (last century or so); II: late Holocene-early historical; III: (latest Pleistocene-) middle Holocene

each recognized unit should be carefully considered in this type of analysis. Furthermore, as above discussed, the unit of abandoned channels includes both high sinuosity cut-off reaches developed during a meandering stage of the alluvial plain and low sinuosity ones, associated to a river system characterized by a “braided” pattern.

5 Discussion

5.1 Need for a detailed geomorphological mapping

For the purpose of a geotechnical study in an earthquake-prone country, the liquefaction susceptibility of sediments must be initially assessed on a regional scale. To accomplish this task, geologists and engineers use criteria related to the first order geomorphological characteristics and the general depositional environment associated to the shallow sediments like, for example, fluvial, lacustrine, coastal, etc. The most applied and well-known classifications are the ones proposed by Youd and Perkins (1978), Wakamatsu (1992) and recently by Wakamatsu et al. (2001). The former approach (Youd and Perkins 1978) classified the liquefaction susceptibility of sediments as ‘very low’, ‘low’, ‘moderate’, ‘high’ and ‘very high’ based on their type and age, while the updated version of the latter classification (Wakamatsu et al. 2001) takes into account two levels of ground motion as a proxy for the assessment of liquefaction susceptibility. Specifically, for the worst-case scenario of level 2, the susceptibility to liquefaction of the several geomorphological features is classified as ‘very high’, ‘high’, ‘low’ and ‘none’, while for level 1 scenario the relevant classes are ‘high’, ‘low’, ‘very low’ and ‘none’. In the class of very high susceptibility to liquefaction are included, among others, geomorphological features encountered in the area of Piniada Valley such as abandoned river channels or point bars.

Both classifications are frequently used in the literature and in urban planning for screening the likelihood of geological units to liquefaction and consequently the possible occurrence of liquefaction-induced failures either on the free field and built environment.

This approach highlights the most susceptible areas covered by the relevant type of deposits and it is considered as a basic step for avoiding hazardous locations and/or mitigating the expected failures. In both cases, forecasting of liquefaction occurrences is a procedure that enhances the seismic resilience of the community.

We applied the classification proposed by Youd and Perkins (1978) to Piniada Valley, for examining its effectiveness. According to this classification, the deposited materials of point bars and floodplains are included in the same category as “floodplain deposits”. We also tentatively included the mapped abandoned and drainage channels in the category of the “river channels” proposed by Youd and Perkins (1978) and our ejection cones unit into the “alluvial fan” category of the Authors.

As concerns the age, the categories are: “<500 year” (also referred to as “Recent”), “Holocene” and “Pleistocene”. Correspondence between the Youd and Perkins (1978) categories and the mapped geological units along the Piniada Valley (Fig. 5) are presented in Table 1. Although class III areas have been homogenized into an undifferentiated unit, they mainly represent floodplain surfaces and thus have been labelled in the corresponding Youd and Perkins (1978) category. Our class I unit should be obviously considered as Recent (<500 years), while class IV as Pleistocene. Strictly speaking, both classes II and III are certainly mainly Holocene, but class II partially overlaps the Recent period of Youd and Perkins (1978), while class III their Pleistocene age category.

Based on the classification proposed by Youd and Perkins (1978), the Recent and (Recent-) Holocene floodplain deposits hosted 285 and 121 liquefaction sites, respectively, corresponding to the 53.4% and 22.7% of the total cases of liquefaction phenomena reported along the Piniada Valley. The remaining 23.9% (128 cases) is related to areas characterized as Recent and (Recent-) Holocene river channels category (94 and 34 cases, respectively) of recent and Holocene age, respectively. In terms of density (sites/km²) of liquefaction features for each Youd and Perkins’s (1978) category, Recent and (Recent-) Holocene floodplain areas have 68.2 and 55.0 site/km², respectively, while river channels 64.9 and 15.6 for the two time-windows, respectively (Table 2).

If we consider our geological mapping and introduce in the analysis a distinction between point bars and floodplain surfaces (Fig. 7), we note that the ratio between point bars and floodplain densities for the two younger age categories is relatively high being 8.1 (=60.7/7.5) and 5.1 (=46.0/9.0), respectively. This implies that liquefaction hazard in the two units is quite different. The results therefore suggest the need of refining the Youd and Perkins’ (1978) classification. For example, it would be useful to subdivide the floodplain deposits category into at least point bars and floodplain *sensu stricto*. As a further consequence in introducing such a subdivision, it would be preferable to characterize liquefaction susceptibility for the point bars as very high and high for the Recent and Holocene deposits, respectively, leaving unmodified (i.e. high and moderate, respectively) the degree of susceptibility for the floodplains *s.s.* Our proposal agrees with Wakamatsu et al. (2001), where the point bar deposits are defined as a separate unit and are associated to a very high liquefaction susceptibility in case of level 2 ground motion.

Another issue raised by our geological mapping and the statistical analysis of the 2021 liquefied sites regards the river channels unit. Indeed, all the river channels belonging to class I represent abandoned meanders, while most of those we have included in class II correspond to channels developed during a braided pattern phase of the river system. At this regard, absolute numbers of liquefaction sites (94 vs. 34) and density values (67.1 vs. 15.5 sites/km²) are quite different for the two classes. Although ages (late historical vs. early historical-Late Holocene) could partly justify the difference it is worth to note that meanders are in general deeper than braided channels and therefore the thickness of

Table 2 Degree of liquefaction susceptibility attributed to the mapped units following the classification of the soils proposed by Youd and Perkins (1978)

Geological units (present work)	YP1978			Liquefac- tion sites		Mapped area (km ²)		Lique- faction density sites (km ²)	
I—point bars	R	Floodplain	h	255	285	4.2	8.2	60.7	68.2
I—floodplain				30		4.0		7.5	
I—abandoned channels	R	River channel	vh	94	94	1.4	1.4	67.1	64.9
II—point bars	(R-)H	Floodplain	(h-)m	23	121	0.5	11.4	46.0	55.0
II—floodplain				98		10.9		9.0	
II—abandoned/drainage channels	(R-)H	River channel	(yh-)h	34	34	2.2	2.2	15.5	15.6
III—undifferentiated	H	Floodplain	m	0	0			0	0
IV—cones	Pt	Alluvial fan	l	0	0			0	0

Susceptibility: *vh* very high, *h* high, *m* moderate, *l* low. Age: *R* recent, *(R-)H* recent—Holocene, *H* holocene, *Pt* pleistocene

their infilling is also different along with their potential in terms of liquefaction susceptibility. As a consequence, further detail mapping should be focused on these geological units (abandoned river channels) and it would be desirable to introduce in the future an additional distinction (and susceptibility class subdivision) between low and high sinuosity abandoned river channel reaches (Fig. 5). It is however crucial when performing a liquefaction susceptibility-oriented classification of the abandoned channels to consider also the dominant grain size of the material partially or totally infilling these geomorphological features.

5.2 Lithological heterogeneity on point bars and liquefaction likelihood

A high density of liquefaction phenomena was related to the geomorphological sub-unit of point bars developed in the inner part of meanders, either classified as abandoned cut-off channels or as part of the active riverbed. Although these features could be generally considered as a sand rich area with fractions of finer material, point-bar deposits are laterally discontinuous (Allen 1965) and characterized by a complex distribution of lithofacies (Thomas et al. 1987; Tye 2004; Miall 2006; Durkin et al. 2015; Russell et al. 2018). The grain size of the deposited material is influenced by the flow direction and speed of the water along the meander, with the deposition of the finer grain materials mostly in the downstream part and the coarser ones in the upstream part (Jackson 1976; Fustic et al. 2012; Nardin et al. 2013). This heterogeneity influences the occurrence of liquefaction, as the finer the soil the less susceptible to liquefaction. For the purposes of this study, the method proposed by Russell et al. (2018) was tested with real cases of liquefaction manifestations reported on point bars at the Piniada Valley (Papathanassiou et al. 2022). Specifically, we selected four meander zones (Fig. 8), two related to the main channel of the present-day Pinios River, and two cut-off channels clearly visible on the 1945 aerial photograph of the area, but now obliterated. For each area, the lithological heterogeneity of the point bars was assessed based on the parameters of meander shape and the episodes of meander growth in these features (scroll bars) (Fig. 9).

Application of this methodology required initial measurements regarding the identification of meander apex, the division of the meander into the upstream and downstream limbs, the projection of the thalweg lines and the width of the meander bend (mW), while in cases where scroll bars were visible, the meander migration trajectory (tL) was also projected. Through the first phase, the meander shapes, developed after different growth stages, were classified into four groups of 25 individual shapes based on their geometry (Russell 2017):

- open asymmetric: meanders where the angle between one limb and mW is 90° or greater, as measured on the line of the limb tangent;
- angular: meanders with open triangular shape, where the apex is angular (shape D4 or E2 in Huddleston's classification 1973);
- bulbous: meanders where tangents of their limbs intersect inside the meander shape;
- open symmetric: meanders where the angle between one limb and mW is less than 90° , as measured on the line of the limb tangent.

After classification of the meander shapes, every meander trajectory and its respective apex were drawn separately. Following this, the downstream inflection point was pinpointed for each case as the likely location where a riffle or cross-over once existed, with the cross over segments indicating the occurrence of mud-prone sediments (Smith et al. 2009). Afterwards, meander thalweg lines were subdivided into heterogeneity types of Sand I, Sand II, Mud I, Mud II, according to the relative proportion of coarse- to fine-grained lithology. Generally, heterogeneity types follow a more gradational sequence in open asymmetric, angular, and open symmetric meander shape, by contrast with bulbous shapes. For the first three groups, heterogeneity type Sand-I is mostly recorded on the upstream limb, while Sand-II deposition occurs after the upstream cross-over and varies depending on the geometry of the meander and the point bar growth. Downstream areas, where counter point bars change from concave to convex geometry are characterized by deposition of finer sediments of Mud-I and Mud-II type. On the other hand, bulbous shapes can compound multiple zones of all relative heterogeneity types, due to the existence of more than two inflection points (Carter 2003; Nanson 1980). Combining this knowledge with information regarding the direction or

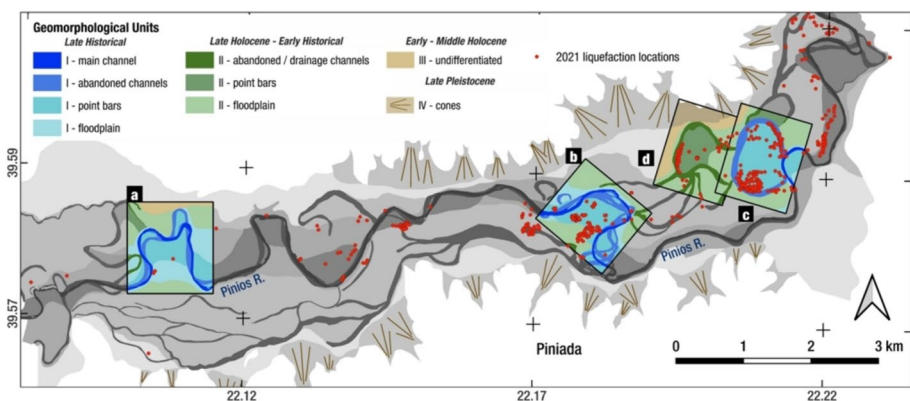


Fig. 8 Map showing the location of the selected meander zones for investigating the sediments distribution

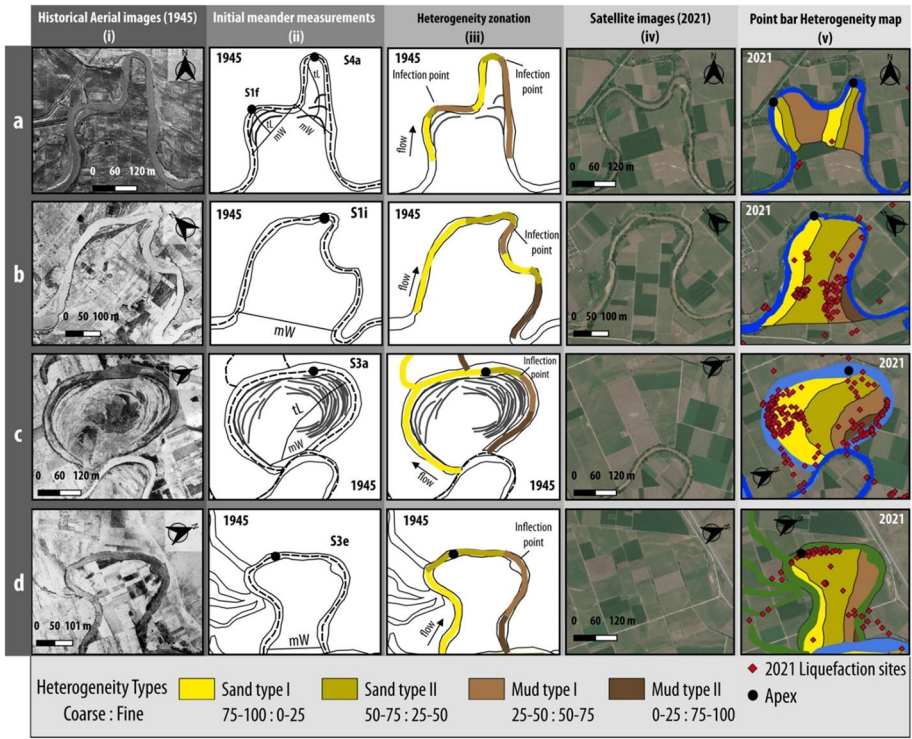


Fig. 9 Assessment of heterogeneity types in four selected meanders (a–d) of the Piniada Valley based on the methodology proposed by Russell (2017) Columns (i–v) represent the different steps of the procedure for evaluating the sedimentary heterogeneity due to the Piniós River evolution from 1945 to 2021. Abbreviations of measurements in column (ii) stand for meander width (*mW*) and meander trajectory length (*tL*), while codes attributed to each meander shape refer to meander shape (*S*); parent group to which the meander belongs (1: open asymmetric, 2: angular, 3: bulbous, 4: open symmetric) and further qualifications of the meander shape (“a” to “i”). See text for more details on the procedure

shifting of scroll bars and cross-cutting relationships resulted in the compilation of a map for each investigated meander showing their relative heterogeneity types.

The first examined meander (a) is located in the western sector of the Piniada Valley (Fig. 9). According to 1945 historical aerial imagery, it was observed that the shape is similar to a compound of two distinct meanders, and it was consequently classified as two open symmetric meander shapes (S4c and S4a). Based on the type of visible scroll bar morphologies it is assumed that the composed point bar results from extensional and rotational movements. Following the meander growth, the recent (2021) satellite image demonstrates the previous compound meander as one of bulbous shape. Due to the projection of two downstream inflection points, the zonation of 1945 and 2021 meander thalweg into heterogeneity types resulted in a map of multiple relative heterogeneity classes. Plotting the liquefaction sites triggered by the 2021 Damasi earthquake it is observed that only one liquefaction event was documented in this point bar.

The second examined meander (b in Fig. 9) is close to the Piniada village, and it has been likely influenced by a growth similar to the previous case. In particular, based on 1945 historical aerial imagery the shape of the meander is similar to a compound of two

distinct meanders, and it was classified as an open asymmetric (S1i) and angular (S2c) meander. According to the 2021 satellite image, the previous compound meander was transformed into a bulbous shape meander (S3e). Tracing of the heterogeneity types in meander thalweg of 1945 and 2021 resulted in a map of four heterogeneity classes, with coarser materials covering the upstream limb and apex area and finer deposits extending in the downstream part. Regarding the 2021 liquefaction records, 56 sites (63.3%) were detected in Sand-I and Sand-II types, and 32 manifestations were reported on the area predominated by finer materials, 29 of them formed in the Mud-I type.

Following the same procedure, we focused on the next meander case where a cut-off shape was formed (c in Fig. 9). Using the historical aerial image of 1945, the meander bend was classified as a bulbous meander, with a rounded apex and not overturned shape (S3a). Based on the type of visible scroll bar morphologies it is assumed that meander growth was extensional and rotational with more than one major directional change. However, due to its abandoned form since 1945, no alterations were detected in the recent 2021 image. Projection of 2021 liquefaction sites show that more than 70% (101 sites) are concentrated in areas characterized by coarser material; 63% (88 sites) and 9.4% (13 sites) detected in Sand-I and Sand-II types respectively.

The fourth area of interest was related to a cut-off meander (d in Fig. 9), formed next to the previous one. Due to its geometry and the existence of older cross-over zones on its upstream limb, in our geological map it has been classified as an older feature, which was initially cut from the former main riverbed and then was partially eroded by the younger meander (3rd case study) associated to a more recent riverbed. Considering that the two cut-off features are not genetically related, we analysed separately the older one and characterized it as a slightly asymmetrical bulbous type (S3e). Based on this evolution and following the former river flow, the meander bend was classified into four heterogeneity types with the Sand-I covering the upstream limb, the Sand-II extending through the apex area and the Mud-I and Mud-II deposited after the inflection point. Regarding the liquefaction phenomena reported in this zone, post-event field observations document that the higher concentration 86% (35 sites) was related to the area considered as Sand-II type.

As a conceptual model, it is expected that the sand prone zones of the meander will be the preferential location for the triggering of liquefaction, while lesser cases should be distributed on the zone predominated by finer (mud) grain size deposits. According to the analysis that took place in this study and shown on Table 3, most of liquefaction occurrences (72,7%) correlated to areas delineated as sand prone, either as Sand I or Sand II, validating the conceptual model in terms of liquefaction potential. The areas classified as

Table 3 Correlation of the spatial distribution of liquefaction sites triggered by the Damasi 2021 earthquake with the relative heterogeneity types of each of the four examined meanders (Fig. 8) analysed in this research

Case study	Heterogeneity type				Liquefaction sites per case
	Sand I	Sand II	Mud I	Mud II	
A	1	0	0	0	1
B	12	44	29	3	88
C	88	13	14	24	139
D	2	35	3	0	40
Liquefaction sites per type	103	92	46	27	268
%	38.4	34.3	17.2	10.1	100.0

mud prone, Mud I and Mud II, hosted instead 73 out of 268 sites, corresponding to approximately the 37%. Despite the finer grain size characteristics of these mud prone areas, they should still be classified as likely to liquefaction, in agreement with several studies of the last 20 years (e.g., Bray and Sancio 2006; Idriss and Boulanger 2008), since even the non-cohesive silty soils of low plasticity are considered as susceptible to liquefaction.

6 Concluding remarks

We have realized a detailed mapping of the late Upper Pleistocene and mainly Holocene deposits outcropping along the Piniada Valley that was largely based on the field and remote sensing observation of geomorphological features, that is to say the geological units (Fig. 5) derive from “above ground” observations and not from geognostic data. Since the beginning of the twentieth century, topographic maps and remote sensing data, either aerial imagery and/or satellite imagery, are commonly available, allowing to improve geological mapping and commonly used for several purposes including hydrogeological and geotechnical studies. During moderate-to-strong seismic events, such maps could better resolve the distribution and the characteristics of the surficial deposits and hence the potential location of earthquake-induced liquefaction phenomena. At this regard, the behaviour of the subsoil layer and the occurrence of liquefaction are basically dictated by the type of predominant material, the general stratigraphic succession and the depth of water table.

The statistical results from the Piniada Valley case study, based on the correlation between the spatial distribution of the liquefaction surface evidence triggered by the 2021 Damasi earthquakes and the mapped geological units (Fig. 7), draw that a refinement of the existing susceptibility classifications is required. Indeed, the present research indicates that the geomorphological feature and geological units most likely to host liquefaction phenomena are the point bars and their deposits. Consequently, it is here proposed to include this type of geomorphology and sediments as a distinct class characterized by a very high susceptibility to liquefaction for material recently deposited, say in the last century or so.

Point bars deposits are developed on meandering fluvial systems where the depositional process is strongly influenced by the river channel. Although the prevailing grain size is represented by sand, the lateral heterogeneity plays a crucial role in determining the liquefaction susceptibility and its potential. If only regional scale geological maps are available, distinguishing or even simply recognizing the different sedimentary facies is quite difficult; for this reason, a detail mapping would become essential for geotechnical purposes and much cheaper relative the performing of numerous boreholes and/or penetrometric tests.

In order to verify and apply this concept to the Piniada Valley case study, we separated sand and mud prone zones within point bar features and compared their spatial distribution with the occurrence of liquefaction cases during the 2021 Damasi earthquakes. This comparison indicates that most liquefaction phenomena occurred in correspondence of sand rich shallow deposits. Thus, it is confirmed that in point bars settings, it is feasible to further detect distinct zones with different liquefaction likelihood. Accordingly, this could improve the existing classification approaches and better forecast the behaviour of soil materials in terms of liquefaction during seismic shaking and thus contribute to reducing the risk of the built environment and enhancing the seismic resilience of a community.

Finally, considering that nowadays it could be feasible for a geologist to trace areas of point bar deposits on a local scale map (e.g., 1:10,000 to 1:50,000), it is strongly recommended to include in any geotechnical investigation for seismic-related purposes the

detailed geological, geomorphological and remote sensing mapping for inferring the presence of these sediments. This in turn could be beneficial for designing structural linear works, like pipelines, motorways, railroad, etc. because the most likely liquefaction areas could be delineated in advance. It is finally highlighted that the proposed procedure is proper for a local-and/or regional-scale providing a more reliable assessment of liquefaction susceptibility and should not substitute the site-specific analyses of liquefaction potential (hazard), which is estimated based on in-situ CPTs and SPTs (e.g., Youd et al. 2001; Cetin et al. 2004; Idriss and Boulanger 2008; etc.).

Supplementary Information The online version contains supplementary material available at <https://doi.org/10.1007/s10518-024-01993-y>.

Acknowledgements We acknowledge the contribution and support of Themistoklis Raptis, Christos Gianakos and many other Piniada residents during the post-seismic field work. We thank the Editor, P. Galli and an anonymous reviewer for their suggestions. The research activities of D.R. are supported by a contract in the frame of the PON REACT EU Project by the Italian MUR (number 09-G-48651-1).

Authorship contributions Conceptualization: SV, RC, GP; methodology: SV, MT, DR; analyses and investigation: SV, MT, DR; writing-original draft preparation: all authors by sections; writing-review and editing: GP, RC, DR; resources: GP, RC, DR; supervision: RC, GP.

Funding Open access funding provided by Università degli Studi di Ferrara within the CRUI-CARE Agreement.

Declarations

Conflict of interest The authors declare that they have no known competing financial interests or personal relationships that could have appeared to influence the work reported in this study. The authors declare also no conflict of interest, ethics, or otherwise.

Informed consent All authors carefully read and approved the final version of the manuscript.

Open Access This article is licensed under a Creative Commons Attribution 4.0 International License, which permits use, sharing, adaptation, distribution and reproduction in any medium or format, as long as you give appropriate credit to the original author(s) and the source, provide a link to the Creative Commons licence, and indicate if changes were made. The images or other third party material in this article are included in the article's Creative Commons licence, unless indicated otherwise in a credit line to the material. If material is not included in the article's Creative Commons licence and your intended use is not permitted by statutory regulation or exceeds the permitted use, you will need to obtain permission directly from the copyright holder. To view a copy of this licence, visit <http://creativecommons.org/licenses/by/4.0/>.

References

- Abayo NI, Caba AC, Chamberlin E, Montoya B (2023) Fluvial geomorphic factors affecting liquefaction-induced lateral spreading. *Earthq Spectra*. <https://doi.org/10.1177/87552930231190655>
- Allen JRL (1965) A review of the origin and characteristics of recent alluvial sediments. *Sedimentology* 5:89–191. <https://doi.org/10.1111/j.1365-3091.1965.tb01561.x>
- Andrews DCA, Martin GR (2000) Criteria for liquefaction of silty soils. In: 12th world conference on earthquake engineering (12WCEE), proceedings, paper no. 0312
- Bastin S, Quigley M, Bassett K (2015) Paleoliquefaction in easter Christchurch, New Zealand. *Geol Soc Am Bull* 12:1348–1365
- Benedetti L, Finkel R, Papanastassiou D, King G, Armijo R, Ryerson F, Farber D, Flerit F (2002) Post-glacial slip history of the Sparta fault (Greece) determined by ³⁶Cl cosmogenic dating: evidence for non-periodic earthquakes. *Geophys Res Lett* 29:1246

- Boulanger RW, Idriss IM (2014) CPT and SPT based liquefaction triggering procedures. Report No. UCD/CGM-14/01 Center for Geotechnical Modeling, Department of Civil and Environmental Engineering, University of California, Davis, USA
- Boulanger RW, Idriss IM (2006) Liquefaction susceptibility criteria for silts and clays. *J Geot Geoenv Eng* 132(11):1413–1426. [https://doi.org/10.1061/\(ASCE\)1090-0241\(2006\)132:11\(1413\)](https://doi.org/10.1061/(ASCE)1090-0241(2006)132:11(1413))
- Bozzoni F, Boni R, Conca D, Lai C, Zuccolo E, Meisina C (2021) Megazonation of earthquake-induced soil liquefaction hazard in continental Europe. *Bull Earthq Eng* 19:4059–4082. <https://doi.org/10.1007/s10518-020-01008-6>
- Bray J, Sancio R (2006) Assessment of the liquefaction susceptibility of fine-grained soils. *J Geotech Geoenviron Eng*. [https://doi.org/10.1061/\(ASCE\)1090-0241\(2006\)132:9\(1165\)](https://doi.org/10.1061/(ASCE)1090-0241(2006)132:9(1165))
- Caputo R (1995) Inference of a seismic gap from geological data: Thessaly (Central Greece) as a case study. *Ann Geofis* 38(1):1–19. <https://doi.org/10.4401/ag-4127>
- Caputo R (2005) Ground effects of large morphogenic earthquakes. *J Geodyn* 40(2–3):113–118. <https://doi.org/10.1016/j.jog.2005.07.001>
- Caputo R, Pavlides S (1993) Late Cainozoic geodynamic evolution of Thessaly and surroundings (Central-Northern Greece). *Tectonophysics* 223(3–4):339–362
- Caputo R, Bravard J-P, Helly B (1994) The Pliocene–quaternary tecto-sedimentary evolution of the Larissa Plain (Eastern Thessaly, Greece). *Geodin Acta* 7(4):219–231
- Caputo R, Monaco C, Tortorici L (2006) Multiseismic cycle deformation rates from Holocene normal fault scarps on Crete (Greece). *Terra Nova* 18(3):181–190
- Caputo R, Catalano S, Monaco C, Romagnoli G, Tortorici G, Tortorici L (2010) Active faulting on the island of Crete (Greece). *Geophys J Int* 183:111–126. <https://doi.org/10.1111/j.1365-246X.2010.04749.x>
- Caputo R, Helly B, Rapti D, Valkaniotis S (2021) Late Quaternary hydrographic evolution in Thessaly (Central Greece): the crucial role of the Piniada Valley. *Quat Int* 635:3–19. <https://doi.org/10.1016/j.quaint.2021.02.013>
- Caputo R, Helly B (2007) The European palaeoseismological museum of Tyrnavos, Central Greece. EGU General Assembly, Vienna, April 16–20, 2007. In: Geophysical research abstract, vol 9, p 00283
- Caputo R, Helly B, Stefani M, Syrides G, Valkaniotis S, Bellesis A, Toufexis G (2022) Description of Peneiada Valley Project-1 borehole. In: Alram E, Gallis K, Toufexis G (eds) Plateia Magoula Zarkou: the Neolithic period, Austrian Academy of Sciences, pp 55–63. ISBN: 978-3-7001-9036-3
- Caputo R (1990) Geological and structural study of the recent and active brittle deformation of the Neogene-Quaternary basins of Thessaly (Central Greece). *Scientific Annals, Aristotle University of Thessaloniki*, 255 pp., 5 encl., 2 vol., Thessaloniki
- Carter DC (2003) 3-D seismic geomorphology: Insights into fluvial reservoir deposition and performance, Widuri field, Java Sea. *AAPG Bull* 87:909–934. <https://doi.org/10.1306/01300300183>
- Cetin KO, Seed RB, Der Kiureghian A, Tokimatsu K, Harder LF Jr, Kayen RE, Moss RES (2004) Standard penetration test-based probabilistic and deterministic assessment of seismic soil liquefaction potential. *ASCE J Geotech Geoenviron Eng* 130(12):1314–1340. [https://doi.org/10.1061/\(ASCE\)1090-0241\(2004\)130:12\(1314\)](https://doi.org/10.1061/(ASCE)1090-0241(2004)130:12(1314))
- Chatzipetros A, Pavlides S, Foumelis M, Sboras S, Galanakis D, Pikridas C, Bitharis S, Kremastas E, Chatzioannou A, Papaioannou I (2021) The northern Thessaly strong earthquakes of March 3 and 4, 2021, and their neotectonic setting. *Bull Geol Soc Greece* 58:222–255. <https://doi.org/10.12681/bgsg.27225>
- Civico R, Brunori CA, De Martini PM, Pucci S, Cinti FR, Pantosti D (2015) Liquefaction susceptibility assessment in fluvial plains using airborne lidar: the case of the 2012 Emilia earthquake sequence area (Italy). *Natl Hazard Earth Syst Sci* 15:2473–2483
- Clark P-U, Dyke AD, Shakun JD, Carlson AE, Clark J, Wohlfarth B, Mitrovica JX, Hostetler SW, McCabe AM (2009) The last glacial maximum. *Science* 325(5941):710–714. <https://doi.org/10.1126/science.1172873>
- De Novellis V, Reale D, Adinolfi GM, Sansosti E, Convetito V (2021) Geodetic model of the March 2021 Thessaly seismic sequence inferred from seismological and InSAR data. *Remote Sens* 13:341. <https://doi.org/10.3390/rs13173410>
- Di Manna P, Guerrieri L, Piccardi L, Vittori E, Castaldini D, Berlusconi A, Bonadeo L, Comerci V, Ferrario F, Gambillara R, Livio F, Lucarini M, Michetti AM (2012) Ground effects induced by the 2012 seismic sequence in Emilia: implications for seismic hazard assessment in the Po Plain. *Ann Geophys* 55(4):697–703. <https://doi.org/10.4401/ag-6143>
- Durkin PR, Hubbard SM, Boyd RL, Leckie DA (2015) Stratigraphic expression of intra-point-bar erosion and rotation. *J Sedim Res* 85:1238–1257. <https://doi.org/10.2110/jsr.2015.78>

- Fustic M, Bennett B, Huang H, Larter S (2012) Differential entrapment of charged oil—new insights on McMurray Formation oil trapping mechanisms. *Mar Petrol Geol* 36(1):50–69. <https://doi.org/10.1016/j.marpetgeo.2012.05.004>
- Galli P (2000) New empirical relationships between magnitude and distance for liquefaction. *Tectonophysics* 324:169–187. [https://doi.org/10.1016/S0040-1951\(00\)00118-9](https://doi.org/10.1016/S0040-1951(00)00118-9)
- Galli P, Castenetti S, Peronace E (2012) May 2012 Emilia earthquakes (Mw 6, northern Italy): macroseismic effects distribution and seismotectonic implications. *Alpine Mediterr Quat* 25(2):105–123
- Ganas A, Valkaniotis S, Briole P, Serpetisdakis A, Kapetanidis V, Karasante I, Kassaras I, Papathanassiou G, Karamitros I, Tsironi V et al (2021) Domino-style earthquakes along normal faults in Northern Thessaly (Greece): Kinematic evidence from field observations, seismology, SAR interferometry and GNSS. *Bull Geol Soc Greece* 58:37–86. <http://dx.doi.org/10.12681/bgsg.27102>
- Hamada M, O'Rourke TD (eds) (1992) Case studies of liquefaction and lifeline performance during past earthquakes, vol 1. Technical Report NCEER-92-0001, State University of New York at Buffalo
- Hellenic Cadastre (2007) Digital surface model. Hellenic Cadastre
- Hellenic Army Geographical Service (2008) Orthophotomaps of 1945–1960
- Huddleston PJ (1973) Fold morphology and some geometrical implications of theories of fold development. *Tectonophysics* 16(1–2):1–46. [https://doi.org/10.1016/0040-1951\(73\)90129-7](https://doi.org/10.1016/0040-1951(73)90129-7)
- Idriss IM, Boulanger RW (2008) Soil liquefaction during earthquakes. In: Monograph MNO-12, Earthquake Engineering Research Institute, Oakland, CA, p 261
- Jackson RG (1976) Sedimentological and fluid-dynamic implications of the turbulent bursting phenomenon in geophysical flows. *J Fluid Mech* 77(3):531–560. <https://doi.org/10.1017/S0022112076002243>
- Karakostas V, Papazachos C, Papadimitriou E, Fouvelis M, Kiratzi A, Pikridas C, Kostoglou A, Kkallas C, Chatzis N, Bitharis S et al (2021) The March 2021 Tyrnavos, central Greece, doublet (Mw6.3 and Mw6.0): Aftershock relocation, faulting details, coseismic slip and deformation. *Bull Geol Soc Greece* 58:131–178
- Kassaras I, Kapetanidis V, Ganas A, Karakonstantis A, Papadimitriou P, Kaviris G, Kouskouna V, Voulgaris N (2022) Seismotectonic analysis of the 2021 Damasi-Tyrnavos (Thessaly, Central Greece) earthquake sequence and implications on the stress field rotations. *J Geodyn* 150:101898. <https://doi.org/10.1016/j.jog.2022.101898>
- Kaviris G (2023) Shear-wave splitting perspectives from the intense aftershock sequence of Damasi—Tyrnavos. *Ann Geophys* 66(2):1–15. <https://doi.org/10.4401/ag-8848>
- Koukouvelas IK, Nikolakopoulos KG, Kyriou A, Caputo R, Xypolias P, Mpelesis A, Zygouri V, Verroios S, Apostolopoulos D, Tsentzos I (2021) The March 2021 Damasi earthquake sequence, Central Greece: reactivation evidence across the westward propagating Tyrnavos Graben. *Geosciences* 11:328. <https://doi.org/10.3390/geosciences11080328>
- Koukouvelas I, Caputo R, Nikolakopoulos K, Kyriou A, Famiglietti NA (2023) Is the Mesochori Fault a key structure for understanding the earthquake activity during the 2021 Damasi earthquake in the northern Thessaly, Greece? *Geosciences* 13:331. <https://doi.org/10.3390/geosciences13110331>
- Kramer S (2008) Evaluation of liquefaction hazards in Washington State. Washington State Dept. Trans. Rep. WA-RD 668.1
- Mantovani A, Valkaniotis S, Rapti D, Caputo R (2018) Mapping the palaeo-Piniada Valley, Central Greece, based on systematic microtremor analyses. *Pure Appl Geophys* 175:865–881. <https://doi.org/10.1007/s00024-017-1731-7>
- Mason J, Schneiderwind S, Pallikarakis A, Wiatr T, Mechernich S, Papanikolaou I, Reicherter K (2016) Fault structure and deformation rates at the Lastros-Sfaka Graben. *Crete Tectonophysics* 683:216–232. <https://doi.org/10.1016/j.tecto.2016.06.036>
- Meisina C, Boni R, Bozzoni F, Conca D, Perotti C, Persichillo P, Lai CG (2022) Mapping soil liquefaction susceptibility across Europe using the analytic hierarchy process. *Bull Earthq Eng* 20:5601–5632. <https://doi.org/10.1007/s10518-022-01442-8>
- Miall AD (2006) Reconstructing the architecture and sequence stratigraphy of the preserved fluvial record as a tool for reservoir development: a reality check. *AAPG Bull* 90:989–1002
- Michas G, Pavlou K, Avgerinou S-E, Anyfadi E-A, Vallianatos F (2021) Aftershock patterns of the 2021 Mw 6.3 Northern Thessaly (Greece) earthquake. *J Seismol* 26:201–225. <https://doi.org/10.1007/s10950-021-10070-9>
- Moss RES, Chen G (2008) Comparing liquefaction procedures in the U.S. and China. In: 14th World conference on earthquake engineering. Beijing, China, October 12–17
- Nanson GC (1980) Point bar and floodplain formation of the meandering Beatton River, Northeastern British Columbia, Canada. *Sedimentology* 27:3–29. <https://doi.org/10.1111/j.1365-3091.1980.tb01155.x>

- Nardin TR, Howard RF, Carter BJ (2013) Stratigraphic architecture of a large-scale point-bar complex in the McMurray Formation: light detection and ranging and subsurface data integration at Syncrude's Mildred Lake Mine, Alberta, Canada. In: Hein FJ, Leckie DA, Suter JR (eds) Heavy oil and oil sand petroleum systems in Alberta and Beyond. AAPG Studies in Geology, vol 64, pp 273–311
- O'Rourke TD, Hamada M (eds) (1992) Case studies of liquefaction and lifeline performance during past earthquakes, vol 2. Technical Report NCEER-92-0002, State University of New York at Buffalo
- Papadimitriou E, Karakostas V, Papazachos C, Fouvelis M, Kiratzi A, Pikridas C, Bonatis P, Kostoglou A, Kourouklas C, Scordilis E, Bitharis S, Paradisopoulou P, Panou A, Galanis O, Karagianni E, Vamvakaris D, Karagianni I, Kkallas C, Chatzis N, Chatzipetros A, Fotiou A, Ventouzi C, Grendas I, Kementzetzidou D, Karakaisis G, Hatzidimitriou P (2023) The seismogenic structure of March 2021 Tyrnavos (central Greece) doublet (Mw 6.3 and Mw 6.0), constrained by aftershock locations and geodetic data. *Geophys J Int* 235(1):644–689. <https://doi.org/10.1093/gji/ggad253>
- Papanikolaou ID, Roberts GP, Michetti AM (2005) Fault scarps and deformation rates in Lazio-Abruzzo, Central Italy: comparison between geological fault slip-rate and GPS data. *Tectonophysics* 408:147–176
- Papathanassiou G, Pavlides S (2011) GIS-based database of historical liquefaction occurrences in the broader Aegean region, DALO v1.0. *Quat Int* 242:115–125. <https://doi.org/10.1016/j.quaint.2011.03.049>
- Papathanassiou G, Pavlides S, Charstaras B, Pitilakis K (2005) Liquefaction case histories and empirical relations of earthquake magnitude versus distance from the broader Aegean region. *J Geodyn* 40(2–3):257–278. <https://doi.org/10.1016/j.jog.2005.07.007>
- Papathanassiou G, Valkaniotis S, Chaztipetros A, Pavlides S (2010) Liquefaction susceptibility map of Greece. *Bull Geol Soc Greece* 43:1383–1392. <https://doi.org/10.12681/bgsg.11314>
- Papathanassiou G, Caputo R, Rapti-Caputo D (2012) Liquefaction phenomena along the paleo-Reno River caused by the May 20, 2012, Emilia (northern Italy) earthquake. *Ann Geophys* 55(4):735–742. <https://doi.org/10.4401/ag-6147>
- Papathanassiou G, Mantovani A, Tarabusi G, Rapti D, Caputo R (2015) Assessment of liquefaction potential for two liquefaction prone area considering the May 20, 2012 Emilia (Italy) earthquake. *Eng Geol* 189:1–16. <https://doi.org/10.1016/j.enggeo.2015.02.002>
- Papathanassiou G, Valkaniotis S, Ganas A, Stampolidis A, Rapti D, Caputo R (2022) Floodplain evolution and its influence on liquefaction clustering: the case study of March 2021 Thessaly, Greece, seismic sequence. *Eng Geol* 298:1–18. <https://doi.org/10.1016/j.enggeo.2022.106542>
- Polito CP, Martin II JR (2001) Effects of non-plastic fines on the liquefaction resistance of sands. *J Geotech Eng Div* 127:408–415. [https://doi.org/10.1061/\(ASCE\)1090-0241\(2001\)127:5\(408\)](https://doi.org/10.1061/(ASCE)1090-0241(2001)127:5(408))
- Royal Hellenic Army Geographical Service (1909a) Topographic map in scale of 1:75,000, Trikkala sheet
- Royal Hellenic Army Geographical Service (1909b) Topographic map in scale of 1:75,000, Larissa sheet
- Russell CE, Moutney NP, Hodgson DM, Colombera L (2018) A novel approach for prediction of lithological heterogeneity in fluvial point-bar deposits from analysis of meander morphology and scroll-bar pattern. In: Ghinassi M, Colombera L, Moutney NP, Reesink AJH, Bateman M (eds) *Fluvial meanders and their sedimentary products in the rock record*. Wiley, New York. <https://doi.org/10.1002/9781119424437.ch15>
- Russell CE (2017) Prediction of sedimentary architecture and lithological heterogeneity in fluvial point-bar deposits. PhD thesis, University of Leeds, Leeds, UK
- Seed HB, Idriss IM (1982) Ground motions and soil liquefaction during earthquakes. Earthquake Engineering Research Institute, Berkeley, California
- Seed RB, Cetin KO, Moss RES, Kammerer A, Wu J, Pestana J, Riemer M, Sancio RB, Bray JD, Kayen RE, Faris A (2003) Recent advances in soil liquefaction engineering: a unified and consistent framework. In: Keynote presentation, 26th Annual ASCE Los Angeles Geotechnical Spring Seminar, Long Beach, CA
- Smith DG, Hubbard SM, Leckie DA, Fustic M (2009) Counter point bar deposits: lithofacies and reservoir significance in the meandering modern Peace River and ancient McMurray Formation, Alberta, Canada. *Sedimentology* 56:1655–1669
- Taftoglou M, Valkaniotis S, Papathanassiou G, Klimis N, Dokas IA (2022) Detailed liquefaction susceptibility map of Nestos river Delta, Thrace, Greece based on surficial geology and geomorphology. *Geosciences* 12:361. <https://doi.org/10.3390/geosciences12100361>
- Taftoglou M, Valkaniotis S, Karantanellis S, Goula E, Papathanassiou G (2023) Preliminary mapping of liquefaction phenomena triggered by the February 6 2023 M7.7 earthquake, Türkiye/Syria, based on remote sensing data. <https://doi.org/10.5281/zenodo.7668401>
- Thomas RG, Smith DG, Wood JM, Visser J, Calverley-Range EA, Koster EH (1987) Inclined heterolithic stratification-terminology, description, interpretation and significance. *Sed Geol* 53:123–179

- Tokimatsu K, Kazuya H, Hiroko H, Ohno K, Tamura S, Suzuki Y (2019) Liquefaction-induced settlement and tilting of buildings with shallow foundations based on field and laboratory observation. *Soil Dyn Earthq Eng* 124:268–279. <https://doi.org/10.1016/j.soildyn.2018.04.054>
- Tolomei C, Caputo R, Polcari M, Famiglietti NA, Maggini M, Stramondo S (2021) The use of Interferometric Synthetic Aperture Radar for isolating the contribution of major shocks: the case of the March 2021 Thessaly, Greece, seismic sequence. *Geosciences* 11:191. <https://doi.org/10.3390/geosciences11050191>
- Tye RS (2004) Geomorphology: an approach to determining subsurface reservoir dimensions. *AAPG Bull* 88(8):1123–1147. <https://doi.org/10.1306/02090403100>
- Vidakis M (1998) Geological map of Greece in 1:50,000 scale, Map Sheet Farkadona. Institute of Geological & Mineralogical Exploration, Athens, Greece
- Wakamatsu K, Yamamoto A, Tanaka I (2001): Geomorphological criteria for evaluating liquefaction potential considering the level-2 ground motion in Japan. In: Fourth international conference of recent advances in geotechnical earthquake engineering and soil dynamics, San Diego, CA, Proceedings, pp 26–31
- Wakamatsu K (1992) Evaluation of liquefaction susceptibility based on detailed geomorphological classification. In: Proceedings of Annual Meeting Archive Institute, pp 1443–1444
- Wang WS (1979) Some findings in soil liquefaction. Water Conservancy and Hydroelectric Power Scientific Research Institute, Beijing, China
- Wotherspoon L, Pender M, Orense RP (2012) Relationship between observed liquefaction at Kaiapoi following the 2010 Darfield earthquake and former channels of the Waimakariri River. *Eng Geol* 125:45–55. <https://doi.org/10.1016/j.enggeo.2011.11.001>
- Youd TL, Perkins DM (1978) Mapping of liquefaction induced ground failure potential. *J Geotech Eng Div* 104:433–446
- Youd TL, Idriss IM, Andrus RD, Arango I, Castro G, Christian JT, Dobry R, Finn WDL, Harder LF, Hynes ME, Ishihara K, Koester JP, Liao SSC, Marcuson WF, Martin GR, Mitchell JK, Moriwaki Y, Power MS, Robertson PK, Seed RB, Stokoe KH (2001) Liquefaction resistance of soils: Summary report from the 1996 NCEER and 1998 NCEER/NSF workshops on evaluation of liquefaction resistance of soils. *J Geotech Geoenviron Eng* 127(10):817–833. [https://doi.org/10.1061/\(ASCE\)1090-0241\(2001\)127:4\(297\)](https://doi.org/10.1061/(ASCE)1090-0241(2001)127:4(297))
- Youd TL (1993) Liquefaction-induced lateral spread displacement. Naval Civil Engineering Laboratory
- Youd TL (1998) Screening guide for rapid assessment of liquefaction hazard at highway bridge sites. Technical Report MCEER-98-0005, Multidisciplinary Center for Earthquake Engineering Research, Buffalo New York

Publisher's Note Springer Nature remains neutral with regard to jurisdictional claims in published maps and institutional affiliations.